Tommi Noponen, Dubravko Kičić, Kalle Kotilahti, Timo Kajava, Seppo Kähkönen, Ilkka Nissilä, Pekka Meriläinen, and Toivo Katila. 2005. Simultaneous diffuse near-infrared imaging of hemodynamic and oxygenation changes and electroencephalographic measurements of neuronal activity in the human brain. In: Britton Chance, Robert R. Alfano, Bruce J. Tromberg, Mamoru Tamura, and Eva M. Sevick-Muraca (editors). Optical Tomography and Spectroscopy of Tissue VI. Proceedings of SPIE, volume 5693, pages 179-190.

Simultaneous diffuse near-infrared imaging of hemodynamic and oxygenation changes and electroencephalographic measurements of neuronal activity in the human brain

Tommi Noponen[a,b,c], Dubravko Kičić[b,c], Kalle Kotilahti[a,b,c], Timo Kajava[a], Seppo Kähkönen[c,d], Ilkka Nissilä[a,b,c,d], Pekka Meriläinen[a,b], and Toivo Katila[a,b,c]

[a]Laboratory of Biomedical Engineering, Helsinki University of Technology, Finland
[b]Helsinki Brain Research Center, Helsinki University, Finland
[c]BioMag Laboratory, Helsinki University Central Hospital, Finland
[d]Cognitive Brain Research Unit, Helsinki University, Finland

ABSTRACT

Visually evoked hemodynamic responses and potentials were simultaneously measured using a 16-channel optical imaging instrument and a 60-channel electroencephalography instrument during normo-, hypo- and hypercapnia from three subjects. Flashing and pattern-reversed checkerboard stimuli were used. The study protocol included two counterbalanced measurements during both normo- and hypocapnia and normo- and hypercapnia. Hypocapnia was produced by controlled hyperventilation and hypercapnia by breathing carbon dioxide enriched air. Near-infrared imaging was also used to monitor the concentration changes of oxy- and deoxyhaemoglobin due to hypo- and hypercapnia. Hemodynamic responses and evoked potentials were successfully detected for each subject above the visual cortex. The latencies of the hemodynamic responses during hypocapnia were shorter whereas during hypercapnia they were longer when compared to the latencies during normocapnia. Hypocapnia tended to decrease the latencies of visually evoked potentials compared to those during normocapnia while hypercapnia did not show any consistent effect to the potentials. The developed measurement setup and the study protocol provide the opportunity to investigate the neurovascular coupling and the links between the baseline level of blood flow, electrical activity and hemodynamic responses in the human brain.

Keywords: Diffuse near-infrared imaging, hemodynamic responses, EEG, visually evoked potentials, hypercapnia, hypocapnia

1. INTRODUCTION

Electroencephalography (EEG) is an established method to measure neuronal activity in the human brain. [1] It is a versatile technique for clinical and neuroscientific studies but does not provide direct information on hemodynamic and oxygenation changes in tissue. On the other hand, diffuse near-infrared spectroscopic imaging (NIRSI) allows one to measure local concentration changes in oxygenated ($\Delta[\mathrm{HbO_2}]$) and deoxygenated haemoglobin ($\Delta[\mathrm{HbR}]$), which are crucial elements when studying hemodynamic and oxygenation processes in the human brain. The neuronal and vascular processes in the brain are linked together by the so-called neurovascular coupling. [2,3]

Here, NIRSI and EEG measurements are combined to study neuronal, vascular and metabolic changes simultaneously in the human brain. In this way we obtain more comprehensive information on brain functions than information obtained just using a single method and have the possibility to study the neurovascular coupling. Visual stimuli were used to evoke event-related brain activities.

Carbon dioxide ($\mathrm{CO_2}$) is a major regulator of cerebral blood flow (CBF) in the human brain. [4] Generally, hypocapnia decreases CBF whereas hypercapnia increases it. During stimulation, the baseline level of CBF was changed by adjusting the $\mathrm{CO_2}$ content of the inhaled and exhaled air. This arrangement makes it possible to study the effects of hypo- and hypercapnia on the optical and electrical responses and to reveal possible links between the baseline of CBF and/or neuronal and vascular responses of the brain.

Further author information:
Send correspondence to T.N., E-mail: tommi.noponen@hut.fi, Telephone: 358 9 451 5838

Optical Tomography and Spectroscopy of Tissue VI, edited by Britton Chance, Robert R. Alfano, Bruce J. Tromberg, Mamoru Tamura, Eva M. Sevick-Muraca, Proc. of SPIE Vol. 5693 (SPIE, Bellingham, WA, 2005) · 1605-7422/05/$15 · doi: 10.1117/12.588207

The optical imaging studies were carried out using a 16-channel frequency-domain instrument which has been developed at the Helsinki University of Technology.[5] EEG signals were acquired using a 60-channel EEG instrument. The electrodes and optodes were integrated into the same measurement cap to enable the simultaneous measurements.

2. MATERIALS AND METHODS

2.1. Subjects and study design

Measurements were carried out for three male volunteers so that two subjects (Subjects 2 and 3) were measured once and one subject (Subject 1) twice in two separate sessions using different stimuli. During the first session of Subject 1, a radial half-field pattern-reversed checkerboard stimulus (radius = 10 cm) was used. For the other measurements, 16-ms rectangular full-field checkerboard (24x32 cm) flashes were employed. The stimulus was computer controlled and presented on a normal cathode ray tube (CRT) monitor using the Presentation software ® (Version 0.76, Neurobehavioral Systems). The subject was placed approximately 1.4 m from the monitor and the centre of the screen was horizontally aligned for each subject. The stimulus blocks were 4960-ms long with an inter-stimulus interval (ISI) of 496 ms so that each stimulus block contained ten flashes or pattern reverses. The stimulus blocks were separated by 24992-ms rest blocks, during which the monitor showed a constant grey image. During the measurements, the subjects were asked to focus on the small fixation cross in the middle of the screen.

Four measurements were carried out for each subject, two during normo- and hypocapnia and two during normo- and hypercapnia. The measurement series was counterbalanced so that two measurements started with normocapnia and the other started with hypo- or hypercapnia. The order of the measurements was random to minimize the possible effects of the order on the results. Hypocapnia was produced by controlled hyperventilation during which the subject was asked to breath at a normal rate and to use approximately 50% of the maximum ventilation volume. Hypercapnia was produced by breathing CO_2-enriched room air.

The measurement that started with normal breathing had 4-min periods of both normocapnia and hypo- or hypercapnia (Fig. 1b). Recovery from induced hypo- or hypercapnia back to normocapnia takes a few minutes.[4] For this reason hypo- or hypercapnia periods were followed by an 8-min recovery period during which the subject breathed normally (Fig. 1a). This kind of a counterbalanced study protocol makes it possible to minimize other factors which may influence responses

Figure 1. The counterbalanced study protocol. a) A 4-min hypo- or hypercapnia period starts the measurement following by a 8-min period with a normal ventilation. b) In the reversed measurement a 4-min normocapnia period preceded a 4-min hypo- or hypercapnia period.

such as habituation[6] when the responses during normo- and hypo- or hypercapnia are compared. The measurements were carried out at the BioMag Laboratory of the Helsinki University Central Hospital and the ethics committee of the hospital approved the study plan.

2.2. Instrumentation

Our frequency-domain optical imaging instrument has 16 time-multiplexed sources and 16 parallel detection channels. Two source positions and sixteen detection channels were used in this study. The instrument uses a 100-MHz modulation frequency and the measurement is based on the heterodyne technique with a phase-locked loop. The RF signals are mixed into a 5-kHz frequency after which the signals are amplified and acquired into a PC using a 20-kHz sampling frequency. A software lock-in amplifier is used to calculate the modulation amplitude and phase of the optical signals after the measurement. The output filter of the lock-in amplifier had a cut-off frequency of 100 Hz and its output was sampled at a frequency of 500 Hz.

Recently, a new source system with four wavelengths (760, 785, 830, and 850 nm) has been implemented to the imaging instrument.[7] It consists of laser diodes with the light power of 20-60 mW to improve the signal-to-noise ratio (SNR)

of the measurements, fast fiber-optic switches for wavelength and source-position time multiplexing, and a redesigned temperature stabilizer electronics. The new fiber-optic MEMS switches make it possible to measure spatial hemodynamic responses and fast oscillations using several wavelengths. In this study, two wavelengths (760 and 830 nm) with the output powers of approximately 12 and 16 mW, respectively, were employed on the subject's skin.

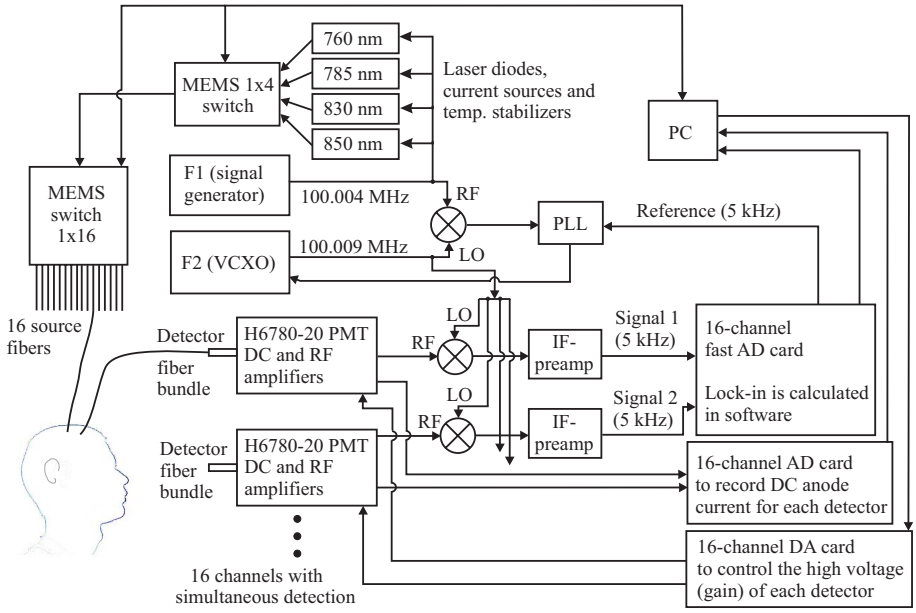

Figure 2. A block diagram of the current implementation of the 16-channel heterodyne frequency-domain instrument.

2.2.1. EEG instrumentation

Continuous EEG signals were recorded using 60 Ag/AgCl electrodes attached to the scalp of the subject. A reference electrode was located on the nose tip. The EEG signals were amplified using a laboratory-made preamplifier compatible with transcranial magnetic stimulation.[8] The pass-band frequency was 0.1-500 Hz and the signals were digitised with 16 bits at a sampling rate of 1450 Hz. Multichannel EEG recordings made it possible for us to localize the strongest EEG activity evoked by the visual stimulus.

2.2.2. EEG and optical imaging cap

To enable simultaneous measurements of optical and EEG responses, the optode holders from the optical imaging instrument were integrated in the EEG cap. The holders contain a piece of thermoplastic on which the PVC sleeves with fiber fixing screws were mounted. The holders were interleaved with the EEG electrodes so that one source fiber was on the left and the other on the right side above visual cortex. The sixteen detection fiber bundles were divided equally on both hemispheres resulting in three different source-to-detector (SD) distances (approximately 35, 42, and 55 mm). Another goal was to form rows containing a source and two detection fiber bundles in a line (e.g., source 1, detectors 12 and 15 in Fig. 3a). Such an arrangement makes it possible to detect signals from different depths at those regions.

2.2.3. Other instrumentation

A Bain breathing system was used to control and measure the CO_2 content of inhaled and exhaled air. The system consists of a gas analyzer, a breathing mask with a tube and connectors for the gas module, a gas bottle, and a rotameter. For hypercapnia measurements, a constant flow level of 6.0 ± 1 l/min of normoxic air mixture with 8% of CO_2 was manually adjusted with the rotameter.

The AS/3 patient monitoring system (Datex-Ohmeda, Finland) was used. It contains a gas monitoring module to measure, e.g., a capnogram with the end-tidal CO_2 ($EtCO_2$) and spirometric parameters such as the ventilation volume. A

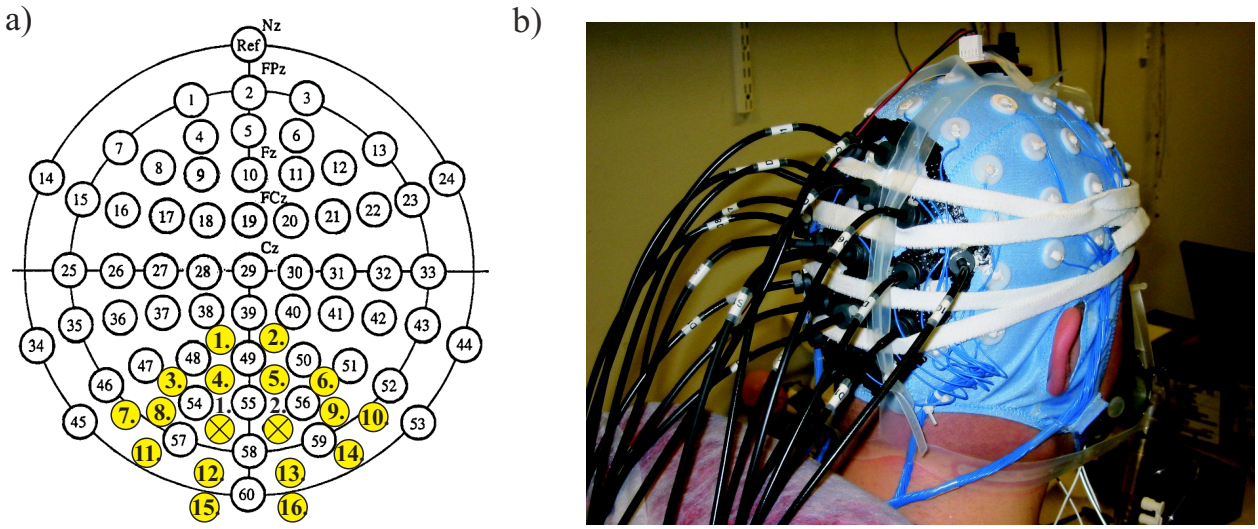

Figure 3. a) The locations of the 60 EEG electrodes, the 2 source optodes (yellow crosses), and the 16 detection optodes (yellow circles with bold-faced numbers). The locations of some electrodes from the International 10-20 electrode placement system are also shown in the picture. b) A photograph of the measurement setup.

hemodynamic module that measures the heart rate (HR) using three-lead electrocardiography and arterial oxygen saturation ($\mathrm{SaO_2}$) using a pulse oximeter is also included.

A two-axis inclinometer chip (SCA100T, VTI Technologies) was taped on the top of subject's head to detect head movements. Both x- and y-signals were digitised with 16 bits at a sampling rate of 9.4 Hz.

2.3. Data processing

2.3.1. Optical signals

Optical data were acquired using an imaging sequence where the two source fibers and two wavelengths were time multiplexed using at least 25-ms long light pulses. The pulses were separated by approximately 15-ms blank intervals. Data were averaged over each pulse resulting in a sampling frequency of approximately 6.2 Hz for the signals from both sources at both wavelengths. The signals from only the closest source were further processed to ensure a reasonable SNR, so that signals from eight detectors were obtained on both hemispheres. The data at different wavelengths were temporally aligned before calculating $\Delta[\mathrm{HbO_2}]$ and $\Delta[\mathrm{HbR}]$ using the modified Beer-Lambert law.[9] Differential pathlength factors of 5.93 at 760 nm and 6.26 at 830 nm were used.[10,11]

Baseline changes of optical signals were extracted by low-pass filtering the signals using a cut-off frequency of 0.0166 Hz. This signal processing made it possible to investigate the changes in $[\mathrm{HbO_2}]$ and $[\mathrm{HbR}]$ due to hypo- and hypercapnia. Then the baseline changes were subtracted from the signals to omit them from further analyses. Baseline corrected signals were again low-pass filtered using a 0.5-Hz cut-off frequency to suppress the pulse and other high-frequency components.

The SNR of changes in $[\mathrm{HbO_2}]$ and $[\mathrm{HbR}]$ due to visual stimuli was improved by averaging the signals over several responses. The averaging window has an approximately 5-s pre-stimulus interval and is approximately 35-s long ending at the beginning of the next stimulus block. The response lengths were equalized by resampling them with respect to the response of maximum length. The responses during normocapnia and hypo- or hypercapnia were averaged separately. From the 12-min data set, responses corresponding to the first and last 4 min of the signals were averaged. This way the eight responses during normocapnia and hypo- or hypercapnia were averaged from each data set.

2.3.2. EEG data

The EEG epochs were also averaged to achieve a better SNR. After rejection of the epochs with pronounced eye movements or blinks, movement artefacts, or muscle activity, the responses were averaged and low-pass filtered with a cut-off frequency

of 40 Hz. The EEG averaging window starts 70 ms before each stimulus and has a total length of 470 ms. Thereby, ten epochs were averaged in each stimulus block provided that none of the epochs were rejected. The stimulus blocks in the data sets were divided into normocapnia and hypo- or hypercapnia intervals as described above. Then 80 epochs of each measurement at most were averaged over normocapnia and hypo- or hypercapnia intervals.

3. RESULTS

3.1. Baseline changes of optical signals during hyper- and hypocapnia

The extracted baselines of optical data were resampled and averaged over different subjects (including the two data sets of Subject 1). Standard errors were calculated over the measurements of different subjects (Fig. 4).

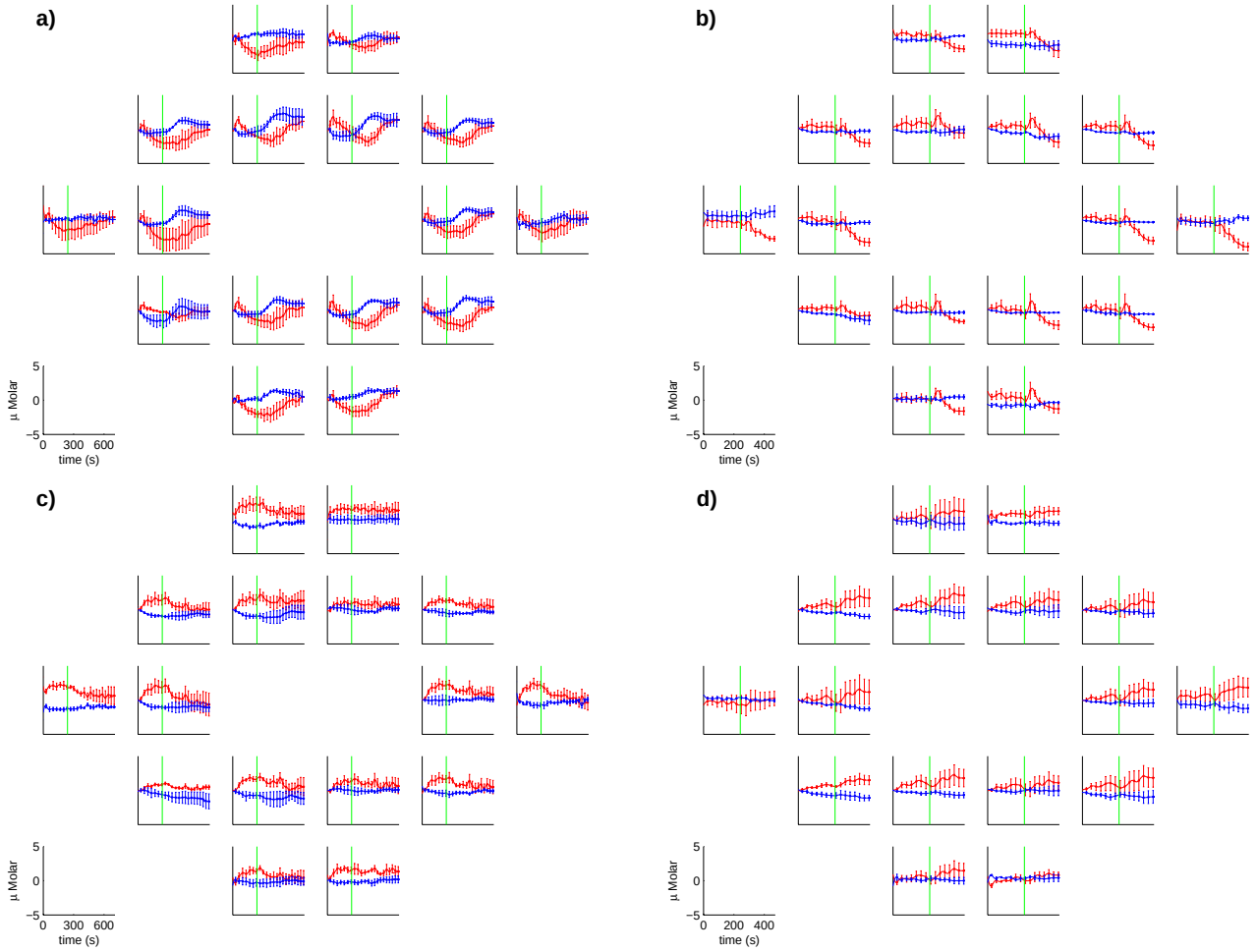

Figure 4. Baseline changes in $[\mathrm{HbO_2}]$ (red curve) and $[\mathrm{HbR}]$ (blue curve) during a) 12-min and b) 8-min hypocapnic measurement, and during c) 12-min and d) 8-min hypercapnic measurement. All the 16 detection channels are shown in the same order as in Fig. 3a. For the 12-min measurements, 4-min hypo- or hypercapnic periods are followed by an 8-min normal breathing periods whereas in 8-min measurements, 4-min hypo- or hypercapnic periods follow 4-min normal breathing periods. The green vertical lines show the switching points in the measurements. The error bars represent the standard errors over the subjects.

The baseline changes in $[\mathrm{HbO_2}]$ were consistent in all the measurements (Fig. 4a-d). During hyperventilation the decrease in $[\mathrm{HbO_2}]$ can be observed in all channels. This reflects the decrease of CBF caused by hypocapnia. During the 8-min recovery period from hypocapnia, $[\mathrm{HbO}_2]$ increases close to its initial level (Fig. 4a). During the 4-min normal

breathing period, the changes in $[HbO_2]$ are minor. During hypercapnia and the corresponding recovery periods, the changes in $[HbO_2]$ are opposite to those during hypocapnic measurements so that hypercapnia increases CBF.

3.2. Optical imaging of visually evoked hemodynamic responses

The visually evoked hemodynamic responses measured using optical imaging could be successfully observed in all the 16 measurements. The strongest responses were found around the channels 8 and 9 in each measurement. Their temporal behaviour was similar to that observed in previous measurements.[12–14] During a response the $[HbO_2]$ typically increases and $[HbR]$ decreases. The peak is reached within 6-12 s from the beginning of stimulus block and response vanishes within 15 s. The upper four channels (channels 3, 4, 5, and 6) typically showed stronger responses than the lower four channels (channels 11, 12, 13, and 14). The SNR of the channels with the 5.5-cm SD separation (channels 1, 2, 7, 10, 15, and 16) was too low to resolve responses.

The responses were further averaged over the entire measurement so that normo- and hypo- or hypercapnic periods were averaged together. Also measurements with the same stimulus were separately averaged together (Fig. 5a-d). This way the SNR was further improved.

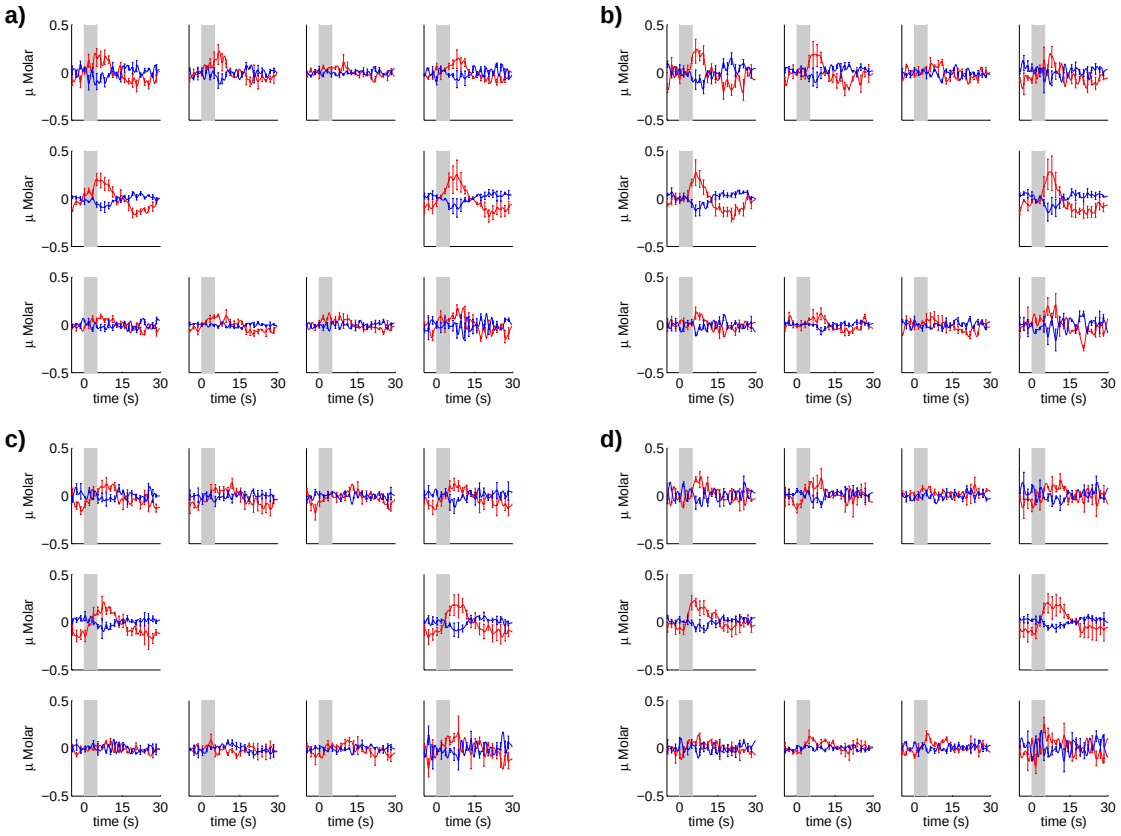

Figure 5. The spatial and temporal behaviour of averaged HbO_2 (red) and HbR (blue) responses. The ten detection channels with the shortest SD separations are shown. The responses are averaged over three subjects and error bars are standard errors between the responses of different subjects. The signals are from the measurements in which a) hypocapnia and b) hypercapnia period starts and b) hypocapnia and d) hypercapnia period ends the measurement.

3.2.1. Hemodynamic responses during hypo- and hypercapnia

The effects of hypo- and hypercapnia on the peak amplitudes and latencies of the HbO_2 responses were investigated. During hypocapnia the peak amplitude of HbO_2 responses was clearly decreased in three, slightly decreased in one, not

significantly changed in three, and slightly increased in one measurement. The limit for clear changes was 0.06 μMolar and for slight change 0.03 μMolar. Also the latency of HbO_2 responses was clearly shorter in five, not significantly changed in two, and slightly longer in one measurement due to hypocapnia. The limits for classifying the latency shifts were 2.0 and 1.0 s, respectively. When all the ten channels, in which the SNR was sufficient to observe the hemodynamic responses, were taken into account, the effects of hypo- and hypercapnia on the responses were typically the strongest on channels 8 and 9. Therefore, further examination was focussed to these channels (Figs. 6a-d and 7a-d).

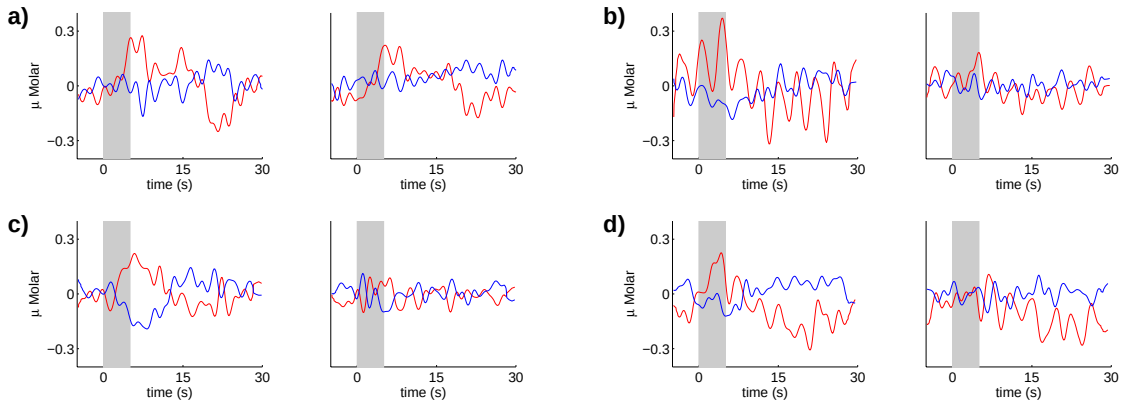

Figure 6. Changes in hemodynamic responses during hypocapnia (Subject 2). Red signals refer to $[HbO_2]$ and blue signals to $[HbR]$. The responses during normocapnia of the measurements in which a hypocapnic period starts (a) and ends (c) the measurement. The responses during hypocapnia of the measurements in which a hypocapnic period starts (b) and ends (d) the measurement. In each image (a)-(d), the signals on the left are from channel 8 and signals on the right are from channel 9. The latency of HbO_2 responses is shorter during hypocapnia.

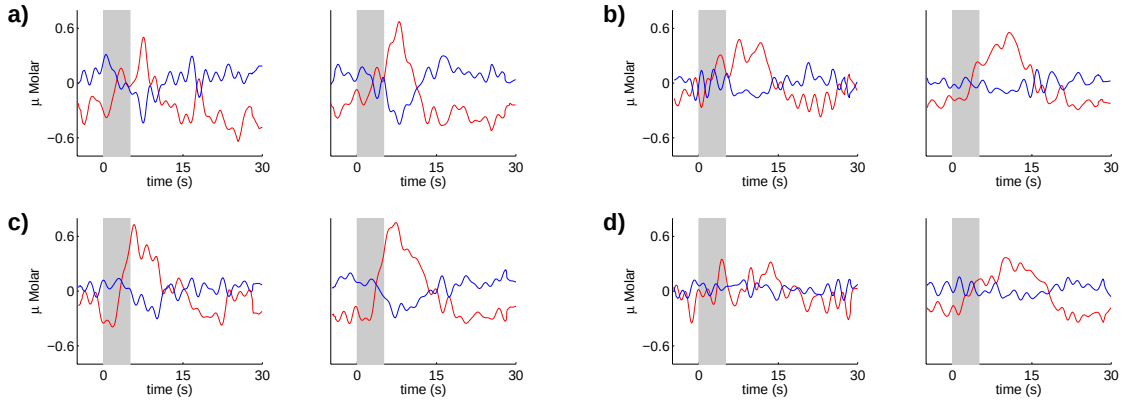

Figure 7. Changes in hemodynamic responses during hypercapnia (Subject 3). Red signals refer to $[HbO_2]$ and blue signals to $[HbR]$. The responses during normocapnia of the measurements in which a hypercapnic period starts (a) and ends (c) the measurement. The responses during hypercapnia of the measurements in which a hypercapnic period starts (b) and ends (d) the measurement. In each image (a)-(d), the signals on the left are from channel 8 and signals on the right are from channel 9. The latency of HbO_2 responses is longer and the peak amplitude shorter during hypercapnia.

The hemodynamic responses during normocapnia and hypercapnia are shown in Fig. 7a-d. During hypercapnia the peak amplitudes of HbO_2 responses were clearly decreased in five, slightly decreased in two, and slightly increased in one measurement. The latency of HbO_2 response was clearly longer in six and slightly longer in two measurements due to hypercapnia. The same limits for the clear and slight amplitude and latency changes were used as before.

3.3. EEG mapping of visually evoked potentials

The visually evoked potentials (VEPs) measured using multi-channel EEG were also analysed. The VEPs were successfully detected in all 16 measurements. The strongest responses were typically found in the ten channels (48-50 and 54-60) located above the visual cortex. The temporal behaviour of responses corresponded to that observed in previous studies and the VEPs had different shapes for the different stimuli.[15] With both stimuli a strong response, often called VEP-P100, around 100 ms from the onset of stimulus was always observed. However, the polarity of the VEP-P100 response was reversed in most of the measurements due to the EEG measurement set-up. In addition, a better SNR was obtained using the full-field flashing stimulus rather than the half-field pattern-reversed stimulus. Besides the strong responses on the visual cortex, evoked potentials spread on other areas of cortex as well. This effect may be caused by the relatively strong stimuli, which in addition to visual perception may induce also other cortical processes. Muscle activity, high level cognitive processing and leakage of strong activity from the relatively large area on visual cortex to the adjacent areas may also induce the response spreading. In Fig. 8, an example of VEPs across the whole head during hypercapnia is shown (Subject 3).

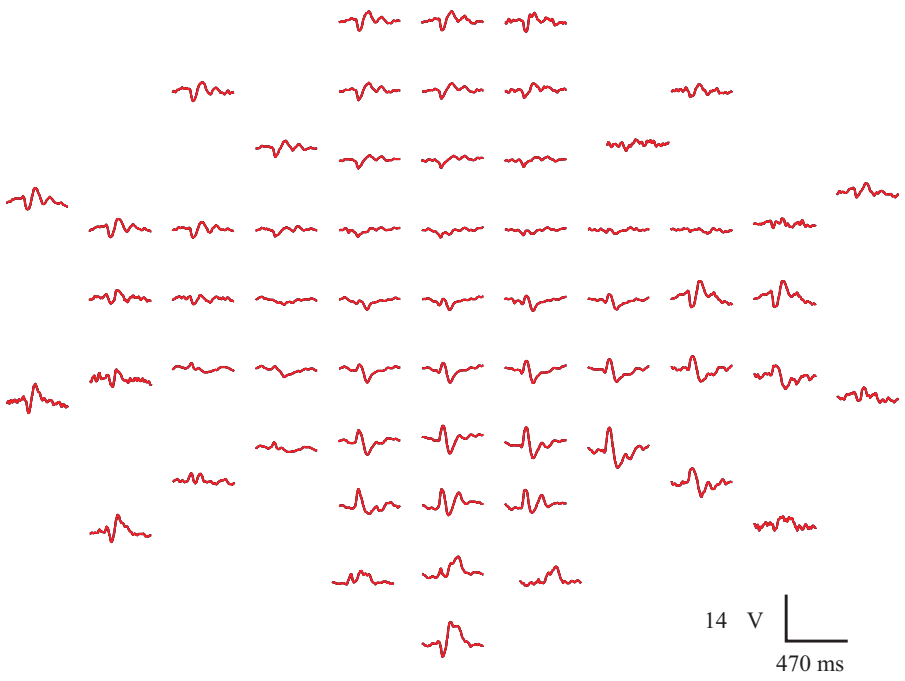

Figure 8. Whole head plot of EEG responses after visual stimulation from Subject 3. The forehead is at the top and back of the head is at the bottom of the picture. Responses are centred on the visual cortex of the occipital lobe even though some of them have spread on the channels on the temporal lobe, especially those on the right side of the picture. However, neither the central areas of the head nor the frontal areas show any strong responses, so that the activity is mainly located at the occipital region. The responses are averaged over the 4-min hypercapnia period, which started the measurement.

3.3.1. Changes of VEPs during hypo- and hypercapnia

The influences of hypo- and hypercapnia to the VEPs were investigated concentrating on changes that occurred in the VEP-P100 components. The analysis focused on changes in the peak amplitudes and latencies of VEP-P100. The peak amplitudes were clearly increased in three, slightly increased in one, not significantly changed in two, and clearly decreased in two measurements due to hypocapnia. The limit for clear change was 1.0 μV and for slight change 0.5 μV. Also the latency of VEP-P100 was clearly shorter in five, slightly shorter in one, not significantly changed in one, and slightly longer in one hypocapnic measurement. The limit for clear latency change was 4 ms and for slight change 2 ms. The changes in VEP-P100 were typically the clearest in the 10 occipital channels (48-50 and 54-60), so that the example results correspond to these channels (Figs. 9a-b). The maximum amplitude and latency changes were determined from channels 58 and 60.

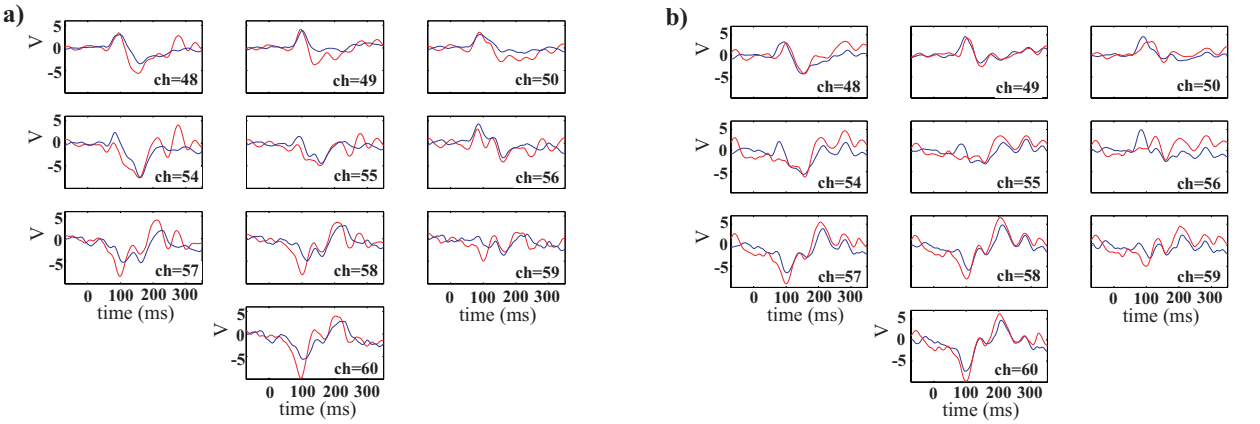

Figure 9. VEPs from the normo- and hypocapnic measurements (Subject 2). The blue lines are recorded during normal breathing while the red lines during hyperventilation. The hypocapnic period was at the beginning (a) or at the end (b) of the measurement. The channels 58 and 60 show a clear increase in the peak amplitude and a reduction in the latency of VEP-P100 due to hypocapnia.

During hypercapnia, the peak amplitudes of VEP-P100 were clearly decreased in two, slightly decreased in two, not significantly changed in one, and increased in two measurements. In one measurement, technical problems prevented the data analysis. The latency of VEP-P100 was clearly shorter in one, slightly shorter in four, not significantly changed in one, slightly longer in one, and clearly longer in one measurement. The same limits for the clear and slight amplitude and latency changes were used as above. The ten occipital channels (48-50 and 54-60) are again used to show the changes in VEP-P100 during hypercapnia because of the pronounced changes in the signals of these channels (Figs. 10a-b).

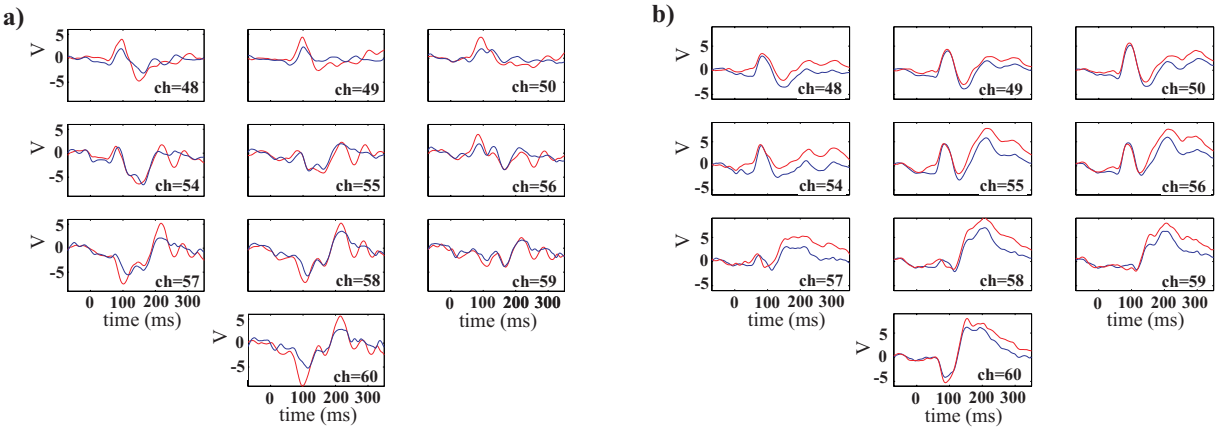

Figure 10. VEPs from the normo- and hypercapnic data sets of Subject 2 (a) and 3 (b). The blue lines are recorded during normal breathing while the red lines during breathing of CO_2-enriched air. The hypercapnic period was at the beginning (a) and at the end (b) of the measurement. In the signals of channels 58 and 60, an increase in the peak amplitude and a reduction in the latency of VEP-P100 due to hypercapnia can be seen.

4. DISCUSSION AND CONCLUSIONS

A new technique to measure VEPs and hemodynamic responses simultaneously with whole-head EEG and multi-channel NIRSI during normo-, hypo-, and hypercapnia was introduced. In previous concomitant NIRSI and EEG measurements, just a single or a few EEG electrodes and a smaller number of optodes than here have been used. [6, 16–18] To the best of our knowledge, visual stimulation has been used only in one earlier concomitant study, where the habituation of visually evoked

neuronal and vascular responses was investigated.[6] In other concomitant studies, an auditory[16] or a semantic stimulus[18] was applied or the baseline signals were investigated.[17] Also, magnetoencephalography and a two-channel near-infrared spectroscopy (NIRS) measurement have been simultaneously recorded during finger movements.[19] Our approach with whole head EEG and multi-channel optical imaging makes it possible, e.g., to localize responses and to find responses with optimum SNR. Simultaneous measurements also provide an effective tool to investigate relationships between neuronal and hemodynamic responses. Hemodynamic and neuronal responses are also measured with concomitant functional magnetic resonance imaging (fMRI) and EEG.[20–24]

In this study, the effect of hypo- and hypercapnia to the hemodynamic responses were measured with NIRSI for the first time. Previous NIRS studies of hypo- and hypercapnia have concentrated only on the baseline changes in $[\mathrm{HbO}_2]$ and $[\mathrm{HbR}]$.[25–27] We found consistent latency shifts of visually evoked hemodynamic responses during hypo- and hypercapnia. The latency shifts also broadened the shape of hemodynamic responses averaged over the whole measurement (Fig. 5). Similar latency shifts have been measured using fMRI,[28] but there the simultaneous VEPs were not recorded. The amplitude changes during hypo- and hypercapnia were not consistent and may even be due to the combined effect of latency shifts and data averaging. The changes in the peak amplitude of hemodynamic responses and changes in the signal contrast due to hypo- and hypercapnia have also been measured with fMRI.[29,30] The measurement of hemodynamic responses during hypo- and hypercapnia makes it possible to investigate, e.g., the links between the different baseline levels of CBF and regional changes in CBF.

NIRSI has several advantages over fMRI in hypo- and hypercapnia measurements and in the combined measurements with the whole-head EEG. Because near-infrared light does not interfere with EEG signals, minimal measurement arrangements and no special data processing methods are required, whereas simultaneous fMRI and EEG experiments, for instance, require relatively advanced arrangements.[20,22] NIRSI instruments are also portable and the method does not require magnetic shielding, so that complex study paradigms and measurements in special environments become possible. NIRSI provides information on the changes in $[\mathrm{HbO}_2]$ as well and it can be used to measure baseline changes during hypo- and hypercapnia simultaneously with hemodynamic responses. By using the EtCO_2 measurement, it is possible to estimate the partial pressure of CO_2 in arterial blood which is related to the level of CBF. In addition, HR and SaO_2 indicate changes in cardiac output and oxygenation of blood. Changes in $[\mathrm{HbO}_2]$ and $[\mathrm{HbR}]$ can provide, however, a direct estimate of impact of hypo- and hypercapnia to the CBF and oxygenation of brain tissue.

The changes in VEPs during hypo- and hypercapnia were also detected. A consistent reduction in the latency of VEP-P100 was observed during hypocapnia. In previous studies, the reduction of latency of VEP-P100[31,32] as well as increase of latency[33] during hyperventilation have been reported. In addition, an increased VEP-P100 amplitude was observed in some measurements during hyperventilation whereas in earlier studies only latency shifts have been reported. The increased peak amplitude cannot be explained by averaging of VEPs with different latencies. As far as we know, the measurements of VEPs during hypercapnia have not been reported. In our measurements, decreases in latencies and increases in VEP-P100 amplitudes during hypercapnia were observed but not consistently. The reason for the inconsistence may be the relatively small number of measurements. A more extensive measurement series is required to explain the changes in VEPs during hypo- and hypercapnia. The presented methods also provide an effective tool to investigate the relationships between the changes of baseline of CBF and VEPs.

The results of this study show that the presented measurement setup provides a promising tool to investigate neurovascular coupling and links between the baseline of CBF and hemodynamic and neuronal responses in the human brain. In addition, the methods may be applied to study physiological processes behind evoked responses and the neurovascular coupling.

ACKNOWLEDGMENTS

Authors like to acknowledge Mrs. Seija Vähä-Vahe for a technical assistant in the preparation of the cap for EEG and optical imaging measurements. This work was financially supported by the Academy of Finland, the National Technology Agency of Finland (Tekes), the Foundation of Technology (TES), the Jenny and Antti Wihuri Foundation, the Emil Aaltonen Foundation, and Instrumentarium Science Foundation.

REFERENCES

1. E. Niedermeyer and F. L. da Silva. *Electroencephalography: Basic Principles, Clinical Applications, and Related Fields*, 4th ed., Williams & Wilkins, Baltimore, 1999.
2. A. Villringer and U. Dirnagl, "Coupling of brain activity and cerebral blood flow: basis of functional neuroimaging," *Cerebrovasc. Brain Metab. Rev.*, **7**, pp. 240-276, 1995.
3. P. J. Magistretti, L. Pellerin, D. L. Rothman, and R. G. Shulman, "Energy on demand," *Science*, **283**, pp. 496-497, 1999.
4. J. F. Nunn, *Applied respiratory physiology*, Butterworths, London, 1987.
5. I. Nissilä, T. Noponen, K. Kotilahti, T. Tarvainen, M. Schweiger, L. Lipiäinen, S. Arridge, and T. Katila, "Instrumentation and calibration methods for the multichannel measurement of phase and amplitude in optical tomography." (submitted to *Rev. Sci. Instrum.*)
6. H. Obrig, H. Israel, M. Kohl-Bareis, K. Uludag, R. Wenzel, B. Muller, G. Arnold, and A. Villringer, "Habituation of the visually evoked potential and its vascular response: implications for neurovascular coupling in the healthy adult," *Neuroimage*, **17**, pp. 1-18, 2002.
7. T. Noponen, *Instrumentation for diffuse optical imaging and near-infrared spectroscopy and their applications in human brain studies*, Licentiate thesis, Helsinki University of Technology, 2004.
8. J. Virtanen, J. Ruohonen, R. Näätänen, and R. J. Ilmoniemi, "Instrumentation for the measurement of electric brain responses to transcranial magnetic stimuli," *Med. Biol. Eng. Comput.*, **37**, pp. 322-326, 1999.
9. D. T. Delpy, M. Cope, P. van der Zee, S. Arridge, S. Wray, and J. S. Wyatt, "Estimation of optical pathlength through tissue from direct time of flight measurement," *Phys. Med. & Biol.*, **33**, pp. 1433-1442, 1988.
10. A. Duncan, J. H. Meek, M. Clemence, C. E. Elwell, L. Tyszchuk, M. Cope, and D. T. Delpy, "Optical pathlength measurements on adult head, calf, and forearm and the head of the newborn infant using phase resolved optical spectroscopy," *Phys. Med. Biol.*, **40**, pp. 295-304, 1995.
11. P. van der Zee, M. Cope, S. R. Arridge, M. Essenpreis, L. A. Potter, and A. D.Edwards, "Experimentally measured optical pathlengths for the adult head, calf and forearm and the head of the newborn infant as a function of interoptode spacing," *Adv. Exp. Med. & Biol.*, **316**, pp. 143-153, 1992.
12. A. Villringer, J. Planck, C. Hock, L. Schleinkofer, and U. Dirnagl, "Near infrared spectroscopy (NIRS): a new tool to study hemodynamic changes during activation of brain function in human adults," *Neurosci. Lett.*, **154**, pp. 101-104, 1993.
13. P. Fransson, G. Kruger, K. D. Merboldt, and J. Frahm, "MRI of functional deactivation: temporal and spatial characteristics of oxygenation-sensitive responses in human visual cortex," *Neuroimage*, **9**, pp. 611-618, 1999.
14. D. A. Soltysik, K. K. Peck, K. D. White, B. Crosson, and R. W. Briggs, "Comparison of hemodynamic response nonlinearity across primary cortical areas," *Neuroimage*, **22**, pp. 1117-1127, 2004.
15. G. F. A. Harding, J. V. Odom, W. Spileers, and H. Spekreijse, "Standard for visual evoked potentials 1995," *Vision Res.* **36**, pp. 3567-3572, 1995.
16. R. P. Kennan, S. G. Horovitz, A. Maki, Y. Yamashita, H. Koizumi, and J. C. Gore. "Simultaneous recording of event-related auditory oddball response using transcranial near infrared optical topography and surface EEG," *Neuroimage*, **16**, pp. 587-592, 2002.
17. M. Moosmann, P. Ritter, I. Krastel, A. Brink, S. Thees, F. Blankenburg, B. Taskin, H. Obrig, and A. Villringer, "Correlates of alpha rhythm in functional magnetic resonance imaging and near infrared spectroscopy," *Neuroimage*, **20**, pp. 145-158, 2003.
18. S. G. Horovitz and J. C. Gore, "Simultaneous event-related potential and near-infrared spectroscopic studies of semantic processing," *Hum. Brain Mapp.*, **22**:110-115, 2004.
19. B. M. Mackert, G. Wubbeler, S. Leistner, K. Uludag, H. Obrig, A. Villringer, L. Trahms, and G. Curio, "Neurovascular coupling analyzed non-invasively in the human brain," *Neuroreport*, **15**, pp. 63-66, 2004.
20. G. Bonmassar, N. Hadjikhani, J. R. Ives, D. Hinton, and J. W. Belliveau, "Influence of EEG electrodes on the BOLD fMRI signal," *Hum. Brain Mapp.*, **14**, pp. 108-115, 2001.
21. G. Bonmassar, D. P. Schwartz, A. K. Liu, K. K. Kwong, A. M. Dale, and J. W. Belliveau, "Spatiotemporal brain imaging of visual-evoked activity using interleaved EEG and fMRI recordings," *Neuroimage*, **13**, pp. 1035-1043, 2001.

22. F. Kruggel, C. S. Herrmann, C. J. Wiggins, and D. Y. von Cramon, "Hemodynamic and electroencephalographic responses to illusory figures: recording of the evoked potentials during functional MRI," *Neuroimage*, **14**, pp. 1327-1336, 2001.
23. C. J. Scarff, A. Reynolds, B. G. Goodyear, C. W. Ponton, J. C. Dort, and J. J. Eggermont, "Simultaneous 3-T fMRI and high-density recording of human auditory evoked potentials," *Neuroimage*, **23**, pp. 1129-1142, 2004.
24. C. Mulert, L. Jager, R. Schmitt, P. Bussfeld, O. Pogarell, H. J. Moller, G. Juckel, and U. Hegerl, "Integration of fMRI and simultaneous EEG: towards a comprehensive understanding of localization and time-course of brain activity in target detection," *Neuroimage*, **22**, pp. 83-94, 2004.
25. P. Smielewski, P. Kirkpatrick, P. Minhas, J. D. Pickard, and M. Czosnyka, "Can cerebrovascular reactivity be measured with near-infrared spectroscopy?" *Stroke*, **26**, pp. 2285-2292, 1995.
26. T. J. Germon, P. D. Evans, A. R. Manara., N. J. Barnett, P. Wall, and R. J. Nelson, "Sensitivity of near infrared spectroscopy to cerebral and extra-cerebral oxygenation changes is determined by emitter-detector separation," *J. Clin. Monit. Comput.*, **14**, pp. 353-360, 1998.
27. T. Noponen, M. Paloheimo, P. Meriläinen, T. Kajava, K. Kotilahti, I. Nissilä, and T. Katila, "Multi-channel near-infrared spectroscopy on the human forehead during hypo- and hypercapnia," *OSA Biomedical Topical Meetings and Tabletop Exhibit, Biomedical Optical Spectroscopy and Diagnostics (BOSD)*, paper **WF8**, Miami Beach, Florida, USA, 2004.
28. L. J. Kemna and S. Posse, "Effect of respiratory CO(2) changes on the temporal dynamics of the hemodynamic response in functional MR imaging," *Neuroimage*, **14**, pp. 642-649, 2001.
29. M. Weckesser, S. Posse, U. Olthoff, L. Kemna, S. Dager, and H. W. Muller-Gartner, "Functional imaging of the visual cortex with bold-contrast MRI: hyperventilation decreases signal response," *Magn. Reson. Med.*, **41**, pp. 213-216, 1999.
30. S. Posse, L. J. Kemna, B. Elghahwagi, S. Wiese, and V. G. Kiselev, "Effect of graded hypo- and hypercapnia on fMRI contrast in visual cortex: quantification of T(*)(2) changes by multiecho EPI," *Magn. Reson. Med.*, **46**, pp. 264-271, 2001.
31. H. D. Davies, W. M. Carroll, and F. L. Mastaglia, "Effects of hyperventilation on pattern-reversal visual evoked potentials in patients with demyelination," *J. Neurol. Neurosurg. Psychiatry*, **49**, pp. 1392–1396, 1986.
32. J. Bednarik and O. Novotny, "Value of hyperventilation in pattern-reversal visual evoked potentials," *J. Neurol. Neurosurg. Psychiatry*, **52**, pp. 1107–1109, 1989.
33. V. S. Gavriysky, "Influence of a twofold voluntary hyperventilation on visually evoked cortical potentials and human pupillogram," *Doc. Ophthalmol.*, **77**, pp. 213–224, 1991.